

# Global $\Lambda$ hyperon polarization in nuclear collisions: evidence for the most vortical fluid

The extreme temperatures and energy densities generated by ultra-relativistic collisions between heavy nuclei produce a state of matter with surprising fluid properties<sup>1</sup>. Non-central collisions have angular momentum on the order of  $1000\hbar$ , and the resulting fluid may have a strong vortical structure<sup>2-4</sup> that must be understood to properly describe the fluid. It is also of particular interest because the restoration of fundamental symmetries of quantum chromodynamics is expected to produce novel physical effects in the presence of strong vorticity<sup>15</sup>. However, no experimental indications of fluid vorticity in heavy ion collisions have so far been found. Here we present the first measurement of an alignment between the angular momentum of a non-central collision and the spin of emitted particles, revealing that the fluid produced in heavy ion collisions is by far the most vortical system ever observed. We find that  $\Lambda$  and  $\bar{\Lambda}$  hyperons show a positive polarization of the order of a few percent, consistent with some hydrodynamic predictions<sup>5</sup>. A previous measurement<sup>6</sup> that reported a null result at higher collision energies is seen to be consistent with the trend of our new observations, though with larger statistical uncertainties. These data provide the first experimental access to the vortical structure of the “perfect fluid”<sup>7</sup> created in a heavy ion collision. They should prove valuable in the development of hydrodynamic models that quantitatively connect observations to the theory of the Strong Force. Our results extend the recent discovery<sup>8</sup> of

## **hydrodynamic spin alignment to the subatomic realm.**

The primary objective of the Relativistic Heavy Ion Collider (RHIC) at Brookhaven National Laboratory is to produce a large (relative to the size of a proton) system of matter at temperatures of  $T \approx 200 \text{ MeV}/k_B \approx 2.3 \times 10^{12} \text{ K}$  by colliding gold nuclei traveling at 96.3 – 99.995% of the speed of light. Such temperatures, more than 100,000 times that at the Sun’s core, characterized the universe only a few microseconds after the Big Bang<sup>9</sup>. Under these extreme conditions, the protons and neutrons that comprise our everyday world, melt into a state of deconfined quarks and gluons called the quark-gluon plasma<sup>1,10</sup>. Before RHIC was turned on in 1999, the expectation was that this plasma would be weakly coupled and highly viscous. However, the discovery of strong collective behaviour led to the surprising conclusion that the system generated in these collisions was in fact a liquid with the lowest viscosity ever observed, the “nearly perfect fluid”<sup>7</sup>.

Since then, large teams have undertaken a program of experimental investigation, and increasingly sophisticated hydrodynamic theory has proven remarkably successful in reproducing observed properties of the fluid<sup>11</sup>. A complete understanding of this fluid may provide deep insights into the strongest and most poorly understood of the fundamental forces in nature. Quantum chromodynamics (QCD) is the theory of the strong interactions between quarks and gluons, but experimental input from RHIC is essential to understand quark confinement and the origin of hadron mass.

A collaboration of physicists from 13 countries operates the STAR detector system<sup>12</sup> which

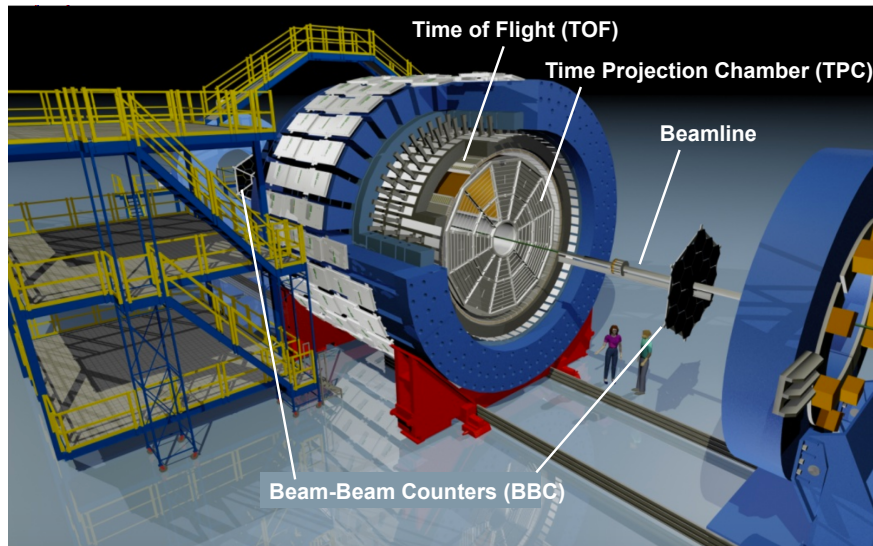


Figure 1: The STAR detector system. Gold nuclei traveling at nearly the speed of light travel along the beamline and collide in the center of the detector system. Charged particles emitted at midrapidity (i.e. having a relatively small component of velocity along the beam direction) are measured in the Time Projection Chamber (see also figure 2) and the Time-of-Flight detectors. Forward- and backward-going fragments are detected in the Beam-Beam Counters.

has recorded billions of collisions at RHIC. A rendering of the STAR experiment is shown in figure 1. Opposing beams of gold nuclei collide in the center of the Time Projection Chamber (TPC), generating a spray of charged particles. The TPC signal from a single event is shown in figure 2. Forward- and backward-traveling particles and fragments that experience only a small deflection are measured in the Beam-Beam Counters.

Most collisions at RHIC are not head-on, and so involve significant angular momentum -of order  $1000\hbar$  for a typical collision. A slight sideward deflection of the forward- and backward-traveling fragments<sup>13</sup> from a given collision allows experimental determination of the direction of

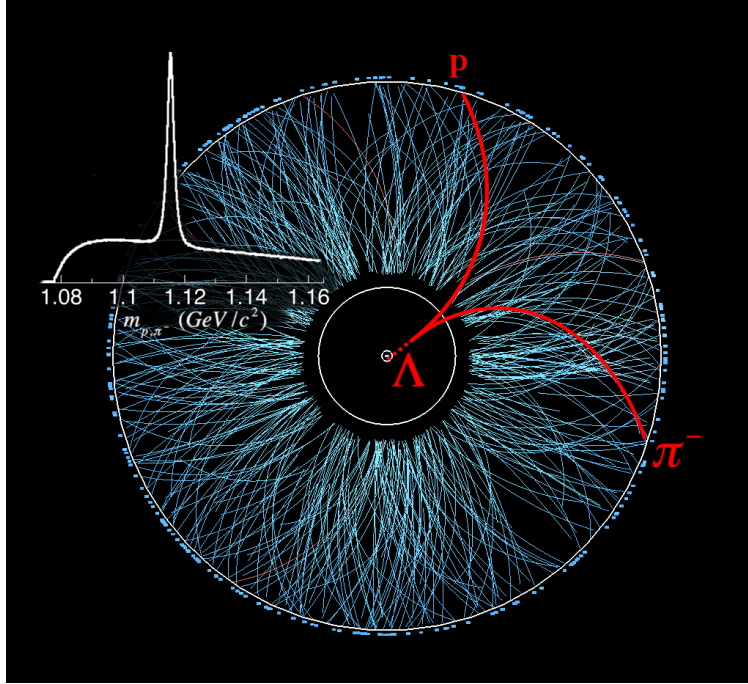


Figure 2: Charged particles from a single Au+Au collision ionize the gas in the TPC, forming tracks that curve in the magnetic field of the detector. The tracks are reconstructed in three dimensions, making them relatively easy to distinguish, but are projected onto a single plane in this figure. As the tracks exit at the outer radius, they leave a signal in the Time-of-Flight (TOF) detector. The species of charged particles is determined by the amount of ionization in the TPC and the flight time as measured by TOF. Charged daughters from the weak decay  $\Lambda \rightarrow p + \pi^-$  are extrapolated backwards, and the parent is identified through topological selection. A clear peak at the  $\Lambda$  mass, obtained by summing over many events, is observed in the invariant-mass distribution, shown in the inset.

the overall angular momentum,  $\hat{J}_{\text{sys}}$ , as shown schematically in figure 3.

Recently, Takahashi *et al.*<sup>8</sup> reported the first observation of a coupling between the vorticity

of a fluid and the internal quantum spin of the electron, opening the door to a new field of fluid spintronics. In their study, vorticity  $\vec{\omega}$ – a measure of the “swirl” of the velocity flow field around any point (non-relativistically,  $\vec{\omega} = \frac{1}{2} \vec{\nabla} \times \vec{v}$ ) – is generated through shear viscous effects as liquid mercury flows next to a rigid wall.

In a heavy ion collision, shear forces generated by the interpenetrating nuclei may present an analogous situation, introducing vorticity to the fluid. Indeed, hydrodynamic calculations predict<sup>14</sup> tremendous vorticity in the fluid at RHIC. So far, no experimental evidence of vorticity at RHIC has been reported, and its role in the fluid evolution has not been explored extensively at the theoretical level.

The vorticity is currently of intense interest, since it is a key ingredient in theories that predict observable effects associated with chiral symmetry restoration and the production of false QCD vacuum states<sup>15</sup>.

Spin-orbit coupling can generate a spin alignment, or polarization, along the direction of the vorticity which is on average parallel to  $\hat{J}_{\text{sys}}$ <sup>2,3</sup>. Thus, polarization measurements of hadrons emitted from the fluid can be used to determine  $\omega \equiv |\vec{\omega}|$ .

It is difficult to measure the spin direction of most hadrons emitted in a heavy ion collision. However  $\Lambda$  and  $\bar{\Lambda}$  hyperons are “self-analyzing.” That is, in the weak decay  $\Lambda \rightarrow p + \pi^-$ , the proton tends to be emitted along the spin direction of the parent  $\Lambda$ <sup>16</sup>. If  $\theta^*$  is the angle between the daughter proton (antiproton) momentum  $\vec{p}_p^*$  and  $\Lambda$  ( $\bar{\Lambda}$ ) polarization vector  $\vec{P}_H$  in the hyperon rest

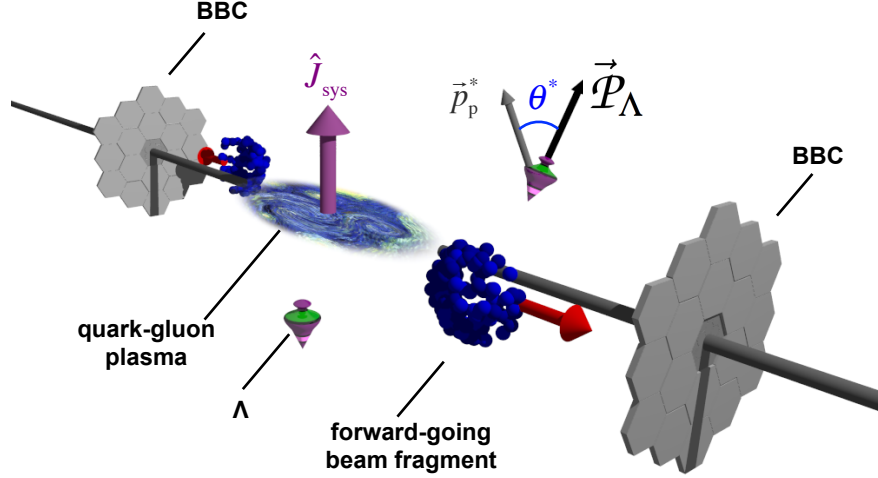


Figure 3: A sketch of the immediate aftermath of a Au+Au collision. The vorticity of fluid created at midrapidity is suggested. The average vorticity points along the direction of the angular momentum of the collision,  $\hat{J}_{\text{sys}}$ . This direction is estimated experimentally by measuring the sideways deflection of the forward- and backward-going fragments and particles in the BBC detectors.  $\Lambda$  hyperons are depicted as spinning tops; see text for details. Obviously, elements in this depiction are not drawn to scale: the fluid and the beam fragments have sizes of a few femtometers, whereas the radius of each BBC is about one meter.

frame, then

$$\frac{dN}{d\cos\theta^*} = \frac{1}{2} \left( 1 + \alpha_{\text{H}} |\vec{P}_{\text{H}}| \cos\theta^* \right). \quad (1)$$

The subscript H denotes  $\Lambda$  or  $\bar{\Lambda}$ , and the decay parameter  $\alpha_{\Lambda} = -\alpha_{\bar{\Lambda}} = 0.642 \pm 0.013^{17}$ . The angle  $\theta^*$  is indicated in figure 3, in which  $\Lambda$  hyperons are depicted as tops spinning about their polarization direction.

The polarization may depend on the momentum of the emitted hyperons. However, when

averaged over all phasespace, symmetry demands that  $\vec{\mathcal{P}}_{\text{H}}$  is parallel to  $\hat{J}_{\text{sys}}$ . Because our limited sample sizes prohibit exploration of these dependences, our analysis assumes that  $\vec{\mathcal{P}}_{\text{H}}$  is independent of momentum, and we extract only an average projection of the polarization on  $\hat{J}_{\text{sys}}$ . This average may be written<sup>6</sup> as

$$\overline{\mathcal{P}}_{\text{H}} \equiv \langle \vec{\mathcal{P}}_{\text{H}} \cdot \hat{J}_{\text{sys}} \rangle = \frac{8}{\pi\alpha_{\text{H}}} \frac{\langle \cos(\phi_p^* - \phi_{\hat{J}_{\text{sys}}}) \rangle}{R_{\text{EP}}^{(1)}}, \quad (2)$$

where  $\phi_{\hat{J}_{\text{sys}}}$  is the azimuthal angle of the angular momentum of the collision,  $\phi_p^*$  is the azimuthal angle of the daughter proton (antiproton) momentum in the  $\Lambda$  frame, and  $R_{\text{EP}}^{(1)}$  is a factor that accounts for the finite resolution with which we determine  $\phi_{\hat{J}_{\text{sys}}}$ <sup>6</sup>. The overline on  $\overline{\mathcal{P}}_{\text{H}}$  and brackets  $\langle \dots \rangle$  denote an average over events and the momenta of  $\Lambda$  hyperons detected in the TPC. Equation 2 is strictly valid only in a perfect detector; angle-dependent detection efficiency leads to a correction factor<sup>6</sup> shifting the results in the present analysis by about 3%.

A relativistic heavy ion collision can produce several hundred charged particles in our detectors. For a given energy, a head-on collision produces the maximum number of emitted particles, while a glancing one produces only a few. To concentrate on collisions with sufficient overlap to produce a fluid with large angular momentum, we select events producing an intermediate number of tracks in the TPC. Twenty percent of all observed collisions produce more tracks than the collisions studied here, while 50% produce fewer; in the parlance of the field, this is known as a 20-50% centrality selection.

Equation 2 quantifies an average alignment between hyperon spin and a global feature of the collision and is hence a “global polarization”<sup>2</sup>. This is distinct from the well-known phe-

nomenon of  $\Lambda$  polarization at very forward angles in proton-proton collisions<sup>18</sup>. The polarization direction from this latter effect depends on  $\Lambda$  momentum and not the global angular momentum; it has zero magnitude at midrapidity.

The solid symbols in figure 4 show our new measurements as a function of collision energy,  $\sqrt{s_{\text{NN}}}$ . At each energy, a positive polarization at the level of 1.1-3.6 times statistical uncertainty is observed for both  $\Lambda$  and  $\bar{\Lambda}$ . Taken in aggregate, the data are statistically consistent with the hypothesis of energy-independent polarizations of  $1.08 \pm 0.15$  and  $1.38 \pm 0.30$  percent for  $\Lambda$  and  $\bar{\Lambda}$ , respectively. Some models predict that the polarization may decrease with collision energy<sup>4,19,20</sup>. While our data is consistent with such a trend, increased statistics would be required to test these predictions definitively. Also shown as open symbols in figure 4 are previously published<sup>6</sup> measurements at  $\sqrt{s_{\text{NN}}} = 62.4$  GeV and 200 GeV. The null result reported in that paper may be seen as consistent with our measurements, within reported statistical uncertainty.

Systematic uncertainties are shown as boxes in the figure and are generally smaller than statistical ones. They are dominated by fluctuations in the estimated combinatoric background of proton-pion pairs whose invariant mass falls within the  $\Lambda$  mass peak, but which do not come from  $\Lambda$  hyperons. Uncertainties due to  $\Lambda$  identification criteria (such as requirements on the spatial proximity of the proton and  $\pi$  daughters) are negligible. There are also small systematic uncertainties in the overall scale, which would scale both the value of  $\bar{\mathcal{P}}_{\text{H}}$  and the statistical uncertainty, thus not affecting the statistical significance of the signal. This includes the uncertainties in the  $\Lambda$  decay parameter  $\alpha$  (2%)<sup>17</sup>, the reaction-plane resolution ( $\sim 2\%$ )<sup>21</sup>, and detector efficiency corrections



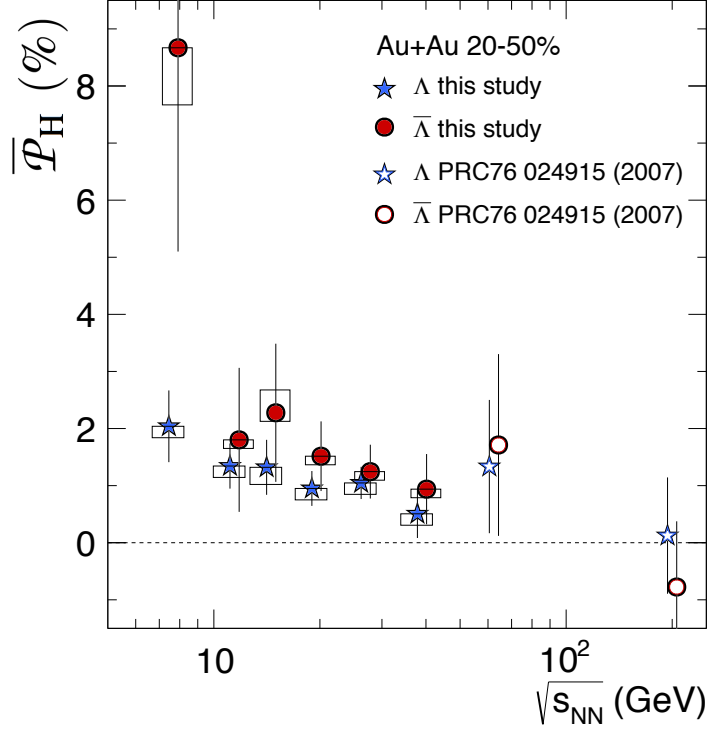


Figure 4: The average polarization  $\bar{P}_H$  (where  $H = \Lambda$  or  $\bar{\Lambda}$ ) from 20-50% central Au+Au collisions is plotted as a function of collision energy. The results of the present study ( $\sqrt{s_{NN}} < 40$  GeV) are shown together with those reported earlier<sup>6</sup> for 62.4 and 200 GeV collisions, for which only statistical errors are plotted. Boxes indicate systematic uncertainties.

( $\sim 3.5\%$ ).

The fluid vorticity may be estimated from the data using the hydrodynamic relation<sup>22</sup>

$$\omega = k_B T (\bar{P}_{\Lambda'} + \bar{P}_{\bar{\Lambda}'}) / \hbar, \quad (3)$$

where  $T$  is the temperature of the fluid at the moment when particles are emitted from it. The subscripts ( $\Lambda'$  and  $\bar{\Lambda}'$ ) in equation 3 indicate that these polarizations are for “primary” hyperons emitted directly from the fluid. However, most of the  $\Lambda$  and  $\bar{\Lambda}$  hyperons at these collision ener-

gies are not primary, but are decay products from heavier particles (e.g.  $\Sigma^{*,+} \rightarrow \Lambda + \pi^+$ ), which themselves would be polarized by the fluid. The data in figure 4 contain both primary and these “feed-down” contributions. At these collision energies, the effect of feed-down is estimated<sup>22</sup> to produce only  $\sim 20\%$  differences between the polarization of “primary” and “all” hyperons.

The  $\sqrt{s_{\text{NN}}}$ -averaged polarizations indicate a vorticity of  $\omega \approx (9 \pm 1) \times 10^{21} \text{ s}^{-1}$ , with a systematic uncertainty of a factor of 2, mostly due to uncertainties in the temperature. This far surpasses the vorticity of all other known fluids, including solar subsurface flow ( $10^{-7} \text{ s}^{-1}$ )<sup>23</sup>; large-scale terrestrial atmospheric patterns ( $10^{-7} - 10^{-5} \text{ s}^{-1}$ )<sup>24</sup>; supercell tornado cores ( $10^{-1} \text{ s}^{-1}$ )<sup>25</sup>; the Great Red Spot of Jupiter (up to  $10^{-4} \text{ s}^{-1}$ )<sup>26</sup>; and rotating, heated soap bubbles ( $100 \text{ s}^{-1}$ ) used to model climate change<sup>27</sup>. Vorticities of up to  $150 \text{ s}^{-1}$  have been measured in turbulent flow in bulk superfluid He-II<sup>28</sup>, and Gomez *et al*<sup>29</sup> have recently produced superfluid nanodroplets with  $\omega \approx 10^7 \text{ s}^{-1}$ .

Relativistic heavy ion collisions are expected to produce intense magnetic fields<sup>30</sup> parallel to  $\hat{J}_{\text{sys}}$ . Coupling between the field and the intrinsic magnetic moments of emitted particles may induce a larger polarization for  $\bar{\Lambda}$  than  $\Lambda$  hyperons<sup>22</sup>. This is not inconsistent with our observations, but probing the field will require more data to reduce statistical uncertainties as well as potential effects related to differences in the measured momenta of  $\Lambda$  and  $\bar{\Lambda}$  hyperons.

The discovery of global  $\Lambda$  polarization in non-central heavy ion collisions opens new directions in the study of the hottest, least viscous – and now, most vortical – fluid ever produced in the laboratory. Quantitative estimates of extreme vorticity yield a more complete characterization of

the system and are crucial input to studies of novel phenomena related to chiral symmetry restoration that may provide needed insight into the complex interactions between quarks and gluons.

**Acknowledgements** We thank the RHIC Operations Group and RCF at BNL, the NERSC Center at LBNL, and the Open Science Grid consortium for providing resources and support. This work was supported in part by the Office of Nuclear Physics within the U.S. DOE Office of Science, the U.S. National Science Foundation, the Ministry of Education and Science of the Russian Federation, National Natural Science Foundation of China, Chinese Academy of Science, the Ministry of Science and Technology of China and the Chinese Ministry of Education, the National Research Foundation of Korea, GA and MSMT of the Czech Republic, Department of Atomic Energy and Department of Science and Technology of the Government of India; the National Science Centre of Poland, National Research Foundation, the Ministry of Science, Education and Sports of the Republic of Croatia, and RosAtom of Russia.

1. Adams, J. *et al.* Experimental and theoretical challenges in the search for the quark gluon plasma: The STAR Collaboration's critical assessment of the evidence from RHIC collisions. *Nucl. Phys.* **A757**, 102–183 (2005). nucl-ex/0501009.
2. Liang, Z.-T. & Wang, X.-N. Globally polarized quark-gluon plasma in non-central A+A collisions. *Phys. Rev. Lett.* **94**, 102301 (2005). [Erratum: *Phys. Rev. Lett.*96,039901(2006)], nucl-th/0410079.
3. Becattini, F., Piccinini, F. & Rizzo, J. Angular momentum conservation in heavy ion collisions at very high energy. *Phys. Rev.* **C77**, 024906 (2008). 0711.1253.
4. Pang, L.-G., Petersen, H., Wang, Q. & Wang, X.-N. Vortical Fluid and  $\Lambda$  Spin Correlations in High-Energy Heavy-Ion Collisions. *Phys. Rev. Lett.* **117**, 192301 (2016). 1605.04024.
5. Becattini, F., Csernai, L. & Wang, D. J.  $\Lambda$  polarization in peripheral heavy ion collisions. *Phys. Rev.* **C88**, 034905 (2013). 1304.4427.
6. Abelev, B. I. *et al.* Global polarization measurement in Au+Au collisions. *Phys. Rev.* **C76**, 024915 (2007). 0705.1691.
7. Heinz, U. & Snellings, R. Collective flow and viscosity in relativistic heavy-ion collisions. *Ann. Rev. Nucl. Part. Sci.* **63**, 123–151 (2013). 1301.2826.
8. Takahashi, R. *et al.* Spin hydrodynamic generation. *Nature Physics* **12**, 52–56 (2016).
9. Kolb, E. W. & Turner, M. S. The Early Universe. *Front. Phys.* **69**, 1–547 (1990).

10. Shuryak, E. V. Quantum Chromodynamics and the Theory of Superdense Matter. *Phys. Rept.* **61**, 71–158 (1980).
11. Csernai, L. P. & Stöcker, H. Global collective flow in heavy ion reactions from the beginnings to the future. *J. Phys.* **G41**, 124001 (2014). 1406.1153.
12. Ackermann, K. H. *et al.* STAR detector overview. *Nucl. Instrum. Meth.* **A499**, 624–632 (2003).
13. Voloshin, S. A. & Niida, T. Ultrarelativistic nuclear collisions: Direction of spectator flow. *Phys. Rev.* **C94**, 021901 (2016). 1604.04597.
14. Becattini, F. *et al.* A study of vorticity formation in high energy nuclear collisions. *Eur. Phys. J.* **C75**, 406 (2015). 1501.04468.
15. Kharzeev, D. E., Liao, J., Voloshin, S. A. & Wang, G. Chiral magnetic and vortical effects in high-energy nuclear collisionsA status report. *Prog. Part. Nucl. Phys.* **88**, 1–28 (2016). 1511.04050.
16. Pondrom, L. Hyperon experiments at Fermilab. *Phys. Rep.* **122**, 57 (1985).
17. Olive, K. A. *et al.* Review of Particle Physics. *Chin. Phys.* **C38**, 090001 (2014).
18. Bunce, G. *et al.* Lambda0 Hyperon Polarization in Inclusive Production by 300-GeV Protons on Beryllium. *Phys. Rev. Lett.* **36**, 1113–1116 (1976).
19. Betz, B., Gyulassy, M. & Torrieri, G. Polarization probes of vorticity in heavy ion collisions. *Phys. Rev.* **C76**, 044901 (2007). 0708.0035.

20. Jiang, Y., Lin, Z.-W. & Liao, J. Rotating quark-gluon plasma in relativistic heavy ion collisions. *Phys. Rev.* **C94**, 044910 (2016). 1602.06580.
21. Adamczyk, L. *et al.* Beam-Energy Dependence of the Directed Flow of Protons, Antiprotons, and Pions in Au+Au Collisions. *Phys. Rev. Lett.* **112**, 162301 (2014). 1401.3043.
22. Becattini, F., Karpenko, I., Lisa, M., Uppal, I. & Voloshin, S. Global hyperon polarization at local thermodynamic equilibrium with vorticity, magnetic field and feed-down *submitted to Phys. Rev. C*, (2016). 1610.02506.
23. Komm, R. *et al.* Divergence and vorticity of solar subsurface flows derived from ring-diagram analysis of MDI and GONG data. *Astrophys. J.* **667**, 571–584 (2007).
24. Perry, C. A. Midwestern streamflow, precipitation, and atmospheric vorticity influenced by pacific sea-surface temperatures and total solar-irradiance variations. *Int. J. Clim* **26**, 207–218 (2006).
25. Wurman, J. *et al.* Dual-Doppler analysis of winds and vorticity budget terms near a tornado. *Monthly Weather Review* **135**, 2392–2405 (2007).
26. Choi, D., Banfield, D., Gierasch, P. & Showman, A. Velocity and vorticity measurements of Jupiter’s Great Red Spot using automated cloud feature tracking. *Icarus* **188**, 35–46 (2007).
27. Meuel, T. *et al.* Intensity of vortices: from soap bubbles to hurricanes. *Nature Scientific Reports* **3:3455**, 1–7 (2013).

28. Donnelly, R. Quantized vortices and turbulence in Helium II. *Ann. Rev. Fluid Mech.* **25**, 325–371 (1993).
29. Gomez, L. F. *et al.* Shapes and vorticities of superfluid helium nanodroplets. *Science* **345**, 906–909 (2014). URL <http://science.sciencemag.org/content/345/6199/906>.
30. Skokov, V., Illarionov, A. Yu. & Toneev, V. Estimate of the magnetic field strength in heavy-ion collisions. *Int. J. Mod. Phys.* **A24**, 5925–5932 (2009). 0907.1396.

L. Adamczyk<sup>1</sup>, J. K. Adkins<sup>19</sup>, G. Agakishiev<sup>17</sup>, M. M. Aggarwal<sup>31</sup>, Z. Ahammed<sup>50</sup>, N. N. Ajitanand<sup>40</sup>,  
I. Alekseev<sup>15,26</sup>, D. M. Anderson<sup>42</sup>, R. Aoyama<sup>46</sup>, A. Aparin<sup>17</sup>, D. Arkhipkin<sup>3</sup>, E. C. Aschenauer<sup>3</sup>,  
M. U. Ashraf<sup>45</sup>, A. Attri<sup>31</sup>, G. S. Averichev<sup>17</sup>, X. Bai<sup>7</sup>, V. Bairathi<sup>27</sup>, A. Behera<sup>40</sup>, R. Bellwied<sup>44</sup>,  
A. Bhasin<sup>16</sup>, A. K. Bhati<sup>31</sup>, P. Bhattarai<sup>43</sup>, J. Bielcik<sup>10</sup>, J. Bielcikova<sup>11</sup>, L. C. Bland<sup>3</sup>, I. G. Bordyuzhin<sup>15</sup>,  
J. Bouchet<sup>18</sup>, J. D. Brandenburg<sup>36</sup>, A. V. Brandin<sup>26</sup>, D. Brown<sup>23</sup>, I. Bunzarov<sup>17</sup>, J. Butterworth<sup>36</sup>,  
H. Caines<sup>54</sup>, M. Calderón de la Barca Sánchez<sup>5</sup>, J. M. Campbell<sup>29</sup>, D. Cebra<sup>5</sup>, I. Chakaberia<sup>3</sup>,  
P. Chaloupka<sup>10</sup>, Z. Chang<sup>42</sup>, N. Chankova-Bunzarova<sup>17</sup>, A. Chatterjee<sup>50</sup>, S. Chattopadhyay<sup>50</sup>,  
X. Chen<sup>37</sup>, J. H. Chen<sup>39</sup>, X. Chen<sup>21</sup>, J. Cheng<sup>45</sup>, M. Cherney<sup>9</sup>, W. Christie<sup>3</sup>, G. Contin<sup>22</sup>, H. J. Crawford<sup>4</sup>,  
S. Das<sup>7</sup>, L. C. De Silva<sup>9</sup>, R. R. Debbé<sup>3</sup>, T. G. Dedovich<sup>17</sup>, J. Deng<sup>38</sup>, A. A. Derevschikov<sup>33</sup>,  
L. Didenko<sup>3</sup>, C. Dilks<sup>32</sup>, X. Dong<sup>22</sup>, J. L. Drachenberg<sup>20</sup>, J. E. Draper<sup>5</sup>, L. E. Dunkelberger<sup>6</sup>,  
J. C. Dunlop<sup>3</sup>, L. G. Efimov<sup>17</sup>, N. Elsey<sup>52</sup>, J. Engelage<sup>4</sup>, G. Eppley<sup>36</sup>, R. Esha<sup>6</sup>, S. Esumi<sup>46</sup>,  
O. Evdokimov<sup>8</sup>, J. Ewigleben<sup>23</sup>, O. Eyser<sup>3</sup>, R. Fatemi<sup>19</sup>, S. Fazio<sup>3</sup>, P. Federic<sup>11</sup>, P. Federicova<sup>10</sup>,  
J. Fedorisin<sup>17</sup>, Z. Feng<sup>7</sup>, P. Filip<sup>17</sup>, E. Finch<sup>47</sup>, Y. Fisyak<sup>3</sup>, C. E. Flores<sup>5</sup>, L. Fulek<sup>1</sup>, C. A. Gagliardi<sup>42</sup>,  
D. Garand<sup>34</sup>, F. Geurts<sup>36</sup>, A. Gibson<sup>49</sup>, M. Girard<sup>51</sup>, D. Grosnick<sup>49</sup>, D. S. Gunarathne<sup>41</sup>, Y. Guo<sup>18</sup>,  
A. Gupta<sup>16</sup>, S. Gupta<sup>16</sup>, W. Guryn<sup>3</sup>, A. I. Hamad<sup>18</sup>, A. Hamed<sup>42</sup>, A. Harlenderova<sup>10</sup>, J. W. Harris<sup>54</sup>,  
L. He<sup>34</sup>, S. Heppelmann<sup>32</sup>, S. Heppelmann<sup>5</sup>, A. Hirsch<sup>34</sup>, G. W. Hoffmann<sup>43</sup>, S. Horvat<sup>54</sup>, T. Huang<sup>28</sup>,  
B. Huang<sup>8</sup>, X. Huang<sup>45</sup>, H. Z. Huang<sup>6</sup>, T. J. Humanic<sup>29</sup>, P. Huo<sup>40</sup>, G. Igo<sup>6</sup>, W. W. Jacobs<sup>14</sup>,  
A. Jentsch<sup>43</sup>, J. Jia<sup>3,40</sup>, K. Jiang<sup>37</sup>, S. Jowzaee<sup>52</sup>, E. G. Judd<sup>4</sup>, S. Kabana<sup>18</sup>, D. Kalinkin<sup>14</sup>, K. Kang<sup>45</sup>,  
K. Kauder<sup>52</sup>, H. W. Ke<sup>3</sup>, D. Keane<sup>18</sup>, A. Kechechyan<sup>17</sup>, Z. Khan<sup>8</sup>, D. P. Kikoła<sup>51</sup>, I. Kisel<sup>12</sup>,  
A. Kisiel<sup>51</sup>, L. Kochenda<sup>26</sup>, M. Kocmanek<sup>11</sup>, T. Kollegger<sup>12</sup>, L. K. Kosarzewski<sup>51</sup>, A. F. Kraishan<sup>41</sup>,  
P. Kravtsov<sup>26</sup>, K. Krueger<sup>2</sup>, N. Kulathunga<sup>44</sup>, L. Kumar<sup>31</sup>, J. Kvapil<sup>10</sup>, J. H. Kwasizur<sup>14</sup>, R. Lacey<sup>40</sup>,



J. M. Landgraf<sup>3</sup>, K. D. Landry<sup>6</sup>, J. Lauret<sup>3</sup>, A. Lebedev<sup>3</sup>, R. Lednicky<sup>17</sup>, J. H. Lee<sup>3</sup>, X. Li<sup>37</sup>,  
C. Li<sup>37</sup>, W. Li<sup>39</sup>, Y. Li<sup>45</sup>, J. Lidrych<sup>10</sup>, T. Lin<sup>14</sup>, M. A. Lisa<sup>29</sup>, H. Liu<sup>14</sup>, P. Liu<sup>40</sup>, Y. Liu<sup>42</sup>,  
F. Liu<sup>7</sup>, T. Ljubicic<sup>3</sup>, W. J. Llope<sup>52</sup>, M. Lomnitz<sup>22</sup>, R. S. Longacre<sup>3</sup>, S. Luo<sup>8</sup>, X. Luo<sup>7</sup>, G. L. Ma<sup>39</sup>,  
L. Ma<sup>39</sup>, Y. G. Ma<sup>39</sup>, R. Ma<sup>3</sup>, N. Magdy<sup>40</sup>, R. Majka<sup>54</sup>, D. Mallick<sup>27</sup>, S. Margetis<sup>18</sup>, C. Markert<sup>43</sup>,  
H. S. Matis<sup>22</sup>, K. Meehan<sup>5</sup>, J. C. Mei<sup>38</sup>, Z. W. Miller<sup>8</sup>, N. G. Minaev<sup>33</sup>, S. Mioduszewski<sup>42</sup>,  
D. Mishra<sup>27</sup>, S. Mizuno<sup>22</sup>, B. Mohanty<sup>27</sup>, M. M. Mondal<sup>13</sup>, D. A. Morozov<sup>33</sup>, M. K. Mustafa<sup>22</sup>,  
Md. Nasim<sup>6</sup>, T. K. Nayak<sup>50</sup>, J. M. Nelson<sup>4</sup>, M. Nie<sup>39</sup>, G. Nigmatkulov<sup>26</sup>, T. Niida<sup>52</sup>, L. V. Nogach<sup>33</sup>,  
T. Nonaka<sup>46</sup>, S. B. Nurushev<sup>33</sup>, G. Odyniec<sup>22</sup>, A. Ogawa<sup>3</sup>, K. Oh<sup>35</sup>, V. A. Okorokov<sup>26</sup>, D. Olvitt Jr.<sup>41</sup>,  
B. S. Page<sup>3</sup>, R. Pak<sup>3</sup>, Y. Pandit<sup>8</sup>, Y. Panebratsev<sup>17</sup>, B. Pawlik<sup>30</sup>, H. Pei<sup>7</sup>, C. Perkins<sup>4</sup>, P. Pile<sup>3</sup>,  
J. Pluta<sup>51</sup>, K. Poniatowska<sup>51</sup>, J. Porter<sup>22</sup>, M. Posik<sup>41</sup>, A. M. Poskanzer<sup>22</sup>, N. K. Pruthi<sup>31</sup>, M. Przybycien<sup>1</sup>,  
J. Putschke<sup>52</sup>, H. Qiu<sup>34</sup>, A. Quintero<sup>41</sup>, S. Ramachandran<sup>19</sup>, R. L. Ray<sup>43</sup>, R. Reed<sup>23</sup>, M. J. Rehbein<sup>9</sup>,  
H. G. Ritter<sup>22</sup>, J. B. Roberts<sup>36</sup>, O. V. Rogachevskiy<sup>17</sup>, J. L. Romero<sup>5</sup>, J. D. Roth<sup>9</sup>, L. Ruan<sup>3</sup>,  
J. Rusnak<sup>11</sup>, O. Rusnakova<sup>10</sup>, N. R. Sahoo<sup>42</sup>, P. K. Sahu<sup>13</sup>, S. Salur<sup>22</sup>, J. Sandweiss<sup>54</sup>, M. Saur<sup>11</sup>,  
J. Schambach<sup>43</sup>, A. M. Schmah<sup>22</sup>, W. B. Schmidke<sup>3</sup>, N. Schmitz<sup>24</sup>, B. R. Schweid<sup>40</sup>, J. Seger<sup>9</sup>,  
M. Sergeeva<sup>6</sup>, P. Seyboth<sup>24</sup>, N. Shah<sup>39</sup>, E. Shahaliev<sup>17</sup>, P. V. Shanmuganathan<sup>23</sup>, M. Shao<sup>37</sup>,  
A. Sharma<sup>16</sup>, M. K. Sharma<sup>16</sup>, W. Q. Shen<sup>39</sup>, Z. Shi<sup>22</sup>, S. S. Shi<sup>7</sup>, Q. Y. Shou<sup>39</sup>, E. P. Sichtermann<sup>22</sup>,  
R. Sikora<sup>1</sup>, M. Simko<sup>11</sup>, S. Singha<sup>18</sup>, M. J. Skoby<sup>14</sup>, N. Smirnov<sup>54</sup>, D. Smirnov<sup>3</sup>, W. Solyst<sup>14</sup>,  
L. Song<sup>44</sup>, P. Sorensen<sup>3</sup>, H. M. Spinka<sup>2</sup>, B. Srivastava<sup>34</sup>, T. D. S. Stanislaus<sup>49</sup>, M. Strikhanov<sup>26</sup>,  
B. Stringfellow<sup>34</sup>, T. Sugiura<sup>46</sup>, M. Sumbera<sup>11</sup>, B. Summa<sup>32</sup>, Y. Sun<sup>37</sup>, X. M. Sun<sup>7</sup>, X. Sun<sup>7</sup>,  
B. Surrow<sup>41</sup>, D. N. Svirida<sup>15</sup>, A. H. Tang<sup>3</sup>, Z. Tang<sup>37</sup>, A. Taranenko<sup>26</sup>, T. Tarnowsky<sup>25</sup>, A. Tawfik<sup>53</sup>,  
J. Thäder<sup>22</sup>, J. H. Thomas<sup>22</sup>, A. R. Timmins<sup>44</sup>, D. Tlusty<sup>36</sup>, T. Todoroki<sup>3</sup>, M. Tokarev<sup>17</sup>, S. Trentalange<sup>6</sup>,

R. E. Tribble<sup>42</sup>, P. Tribedy<sup>3</sup>, S. K. Tripathy<sup>13</sup>, B. A. Trzeciak<sup>10</sup>, O. D. Tsai<sup>6</sup>, T. Ullrich<sup>3</sup>, D. G. Underwood<sup>2</sup>, I. Upsal<sup>29</sup>, G. Van Buren<sup>3</sup>, G. van Nieuwenhuizen<sup>3</sup>, A. N. Vasiliev<sup>33</sup>, F. Videbæk<sup>3</sup>, S. Vokal<sup>17</sup>, S. A. Voloshin<sup>52</sup>, A. Vossen<sup>14</sup>, G. Wang<sup>6</sup>, Y. Wang<sup>7</sup>, F. Wang<sup>34</sup>, Y. Wang<sup>45</sup>, J. C. Webb<sup>3</sup>, G. Webb<sup>3</sup>, L. Wen<sup>6</sup>, G. D. Westfall<sup>25</sup>, H. Wieman<sup>22</sup>, S. W. Wissink<sup>14</sup>, R. Witt<sup>48</sup>, Y. Wu<sup>18</sup>, Z. G. Xiao<sup>45</sup>, W. Xie<sup>34</sup>, G. Xie<sup>37</sup>, J. Xu<sup>7</sup>, N. Xu<sup>22</sup>, Q. H. Xu<sup>38</sup>, Y. F. Xu<sup>39</sup>, Z. Xu<sup>3</sup>, Y. Yang<sup>28</sup>, Q. Yang<sup>37</sup>, C. Yang<sup>38</sup>, S. Yang<sup>3</sup>, Z. Ye<sup>8</sup>, Z. Ye<sup>8</sup>, L. Yi<sup>54</sup>, K. Yip<sup>3</sup>, I. -K. Yoo<sup>35</sup>, N. Yu<sup>7</sup>, H. Zbroszczyk<sup>51</sup>, W. Zha<sup>37</sup>, Z. Zhang<sup>39</sup>, X. P. Zhang<sup>45</sup>, J. B. Zhang<sup>7</sup>, S. Zhang<sup>37</sup>, J. Zhang<sup>21</sup>, Y. Zhang<sup>37</sup>, J. Zhang<sup>22</sup>, S. Zhang<sup>39</sup>, J. Zhao<sup>34</sup>, C. Zhong<sup>39</sup>, L. Zhou<sup>37</sup>, C. Zhou<sup>39</sup>, X. Zhu<sup>45</sup>, Z. Zhu<sup>38</sup>, M. Zyzak<sup>12</sup>

(STAR Collaboration)

<sup>1</sup>AGH University of Science and Technology, FPACS, Cracow 30-059, Poland

<sup>2</sup>Argonne National Laboratory, Argonne, Illinois 60439

<sup>3</sup>Brookhaven National Laboratory, Upton, New York 11973

<sup>4</sup>University of California, Berkeley, California 94720

<sup>5</sup>University of California, Davis, California 95616

<sup>6</sup>University of California, Los Angeles, California 90095

<sup>7</sup>Central China Normal University, Wuhan, Hubei 430079

<sup>8</sup>University of Illinois at Chicago, Chicago, Illinois 60607

<sup>9</sup>Creighton University, Omaha, Nebraska 68178

<sup>10</sup>Czech Technical University in Prague, FNSPE, Prague, 115 19, Czech Republic

<sup>11</sup>Nuclear Physics Institute AS CR, 250 68 Prague, Czech Republic

- <sup>12</sup>Frankfurt Institute for Advanced Studies FIAS, Frankfurt 60438, Germany
- <sup>13</sup>Institute of Physics, Bhubaneswar 751005, India
- <sup>14</sup>Indiana University, Bloomington, Indiana 47408
- <sup>15</sup>Alikhanov Institute for Theoretical and Experimental Physics, Moscow 117218, Russia
- <sup>16</sup>University of Jammu, Jammu 180001, India
- <sup>17</sup>Joint Institute for Nuclear Research, Dubna, 141 980, Russia
- <sup>18</sup>Kent State University, Kent, Ohio 44242
- <sup>19</sup>University of Kentucky, Lexington, Kentucky, 40506-0055
- <sup>20</sup>Lamar University, Physics Department, Beaumont, Texas 77710
- <sup>21</sup>Institute of Modern Physics, Chinese Academy of Sciences, Lanzhou, Gansu 730000
- <sup>22</sup>Lawrence Berkeley National Laboratory, Berkeley, California 94720
- <sup>23</sup>Lehigh University, Bethlehem, PA, 18015
- <sup>24</sup>Max-Planck-Institut für Physik, Munich 80805, Germany
- <sup>25</sup>Michigan State University, East Lansing, Michigan 48824
- <sup>26</sup>National Research Nuclear University MEPhI, Moscow 115409, Russia
- <sup>27</sup>National Institute of Science Education and Research, Bhubaneswar 751005, India
- <sup>28</sup>National Cheng Kung University, Tainan 70101
- <sup>29</sup>Ohio State University, Columbus, Ohio 43210
- <sup>30</sup>Institute of Nuclear Physics PAN, Cracow 31-342, Poland
- <sup>31</sup>Panjab University, Chandigarh 160014, India
- <sup>32</sup>Pennsylvania State University, University Park, Pennsylvania 16802

- <sup>33</sup>Institute of High Energy Physics, Protvino 142281, Russia
- <sup>34</sup>Purdue University, West Lafayette, Indiana 47907
- <sup>35</sup>Pusan National University, Pusan 46241, Korea
- <sup>36</sup>Rice University, Houston, Texas 77251
- <sup>37</sup>University of Science and Technology of China, Hefei, Anhui 230026
- <sup>38</sup>Shandong University, Jinan, Shandong 250100
- <sup>39</sup>Shanghai Institute of Applied Physics, Chinese Academy of Sciences, Shanghai 201800
- <sup>40</sup>State University Of New York, Stony Brook, NY 11794
- <sup>41</sup>Temple University, Philadelphia, Pennsylvania 19122
- <sup>42</sup>Texas A&M University, College Station, Texas 77843
- <sup>43</sup>University of Texas, Austin, Texas 78712
- <sup>44</sup>University of Houston, Houston, Texas 77204
- <sup>45</sup>Tsinghua University, Beijing 100084
- <sup>46</sup>University of Tsukuba, Tsukuba, Ibaraki, Japan,
- <sup>47</sup>Southern Connecticut State University, New Haven, CT, 06515
- <sup>48</sup>United States Naval Academy, Annapolis, Maryland, 21402
- <sup>49</sup>Valparaiso University, Valparaiso, Indiana 46383
- <sup>50</sup>Variable Energy Cyclotron Centre, Kolkata 700064, India
- <sup>51</sup>Warsaw University of Technology, Warsaw 00-661, Poland
- <sup>52</sup>Wayne State University, Detroit, Michigan 48201
- <sup>53</sup>World Laboratory for Cosmology and Particle Physics (WLCAPP), Cairo 11571, Egypt

<sup>54</sup>Yale University, New Haven, Connecticut 06520